

Unexpected Polymorphism in Bromoantimonate(III) Complexes and Its Effect on Optical Properties

Andrey N. Usoltsev, Taisiya S. Sukhikh, Alexander S. Novikov, Vladimir R. Shayapov, Denis P. Pishchur, Ilya V. Korolkov, Ilyas F. Sakhapov, Vladimir P. Fedin, Maxim N. Sokolov, and Sergey A. Adonin*

Cite This: *Inorg. Chem.* 2021, 60, 2797–2804

Read Online

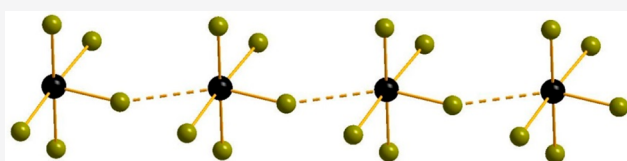
ACCESS |

Metrics & More

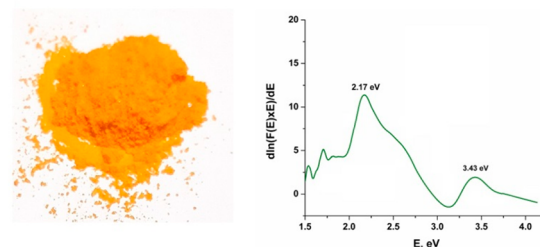
Article Recommendations

Supporting Information

ABSTRACT: Reactions of $[\text{SbBr}_6]^{3-}$ containing HBr solutions with bromide salts of 1,1'-(1,2-ethanediyl)bis(pyridine) (PyC_2^{2+}) or 1,1'-(1,2-ethanediyl)bis(3,5-dimethylpyridine) ($3,5\text{-MePyC}_2^{2+}$) initially result in the formation of the deep orange complexes $\text{Cat}[\text{SbBr}_5]$ (**1** and **2**), featuring unusual $\text{Sb}\cdots\text{Br}$ interactions in the solid state. In the mother liquor, **1** transforms into discrete binuclear $(\text{C}_2\text{Py})_2[\text{Sb}_2\text{Br}_{10}]$, which demonstrates polymorphism (triclinic **3** and monoclinic **4**), while **2** transforms into polymeric $(3,5\text{-MePy})\{[\text{SbBr}_4]\}$ (**5**). DFT calculations reveal that the system of noncovalent $\text{Sb}\cdots\text{Br}$ contacts may be responsible for the appearance of the observed optical properties (unusual deep orange coloring).



Non-covalent interactions cause coloring



INTRODUCTION

Halide complexes, or halometalates, or halogenidometalates (HMs), represent a large class of compounds which is literally as old as coordination chemistry itself.¹ For p-block elements, especially for Pb(II),² Sb(III),³ and Bi(III),^{4,5} they demonstrate an enormous diversity of structural types appearing in the crystalline state: there exist discrete complex anions of different nuclearities^{6–11} (up to 18 for Pb(II)¹²) and one-,^{13–17} two-^{18,19} or even three-dimensional polymers (the latter are known for Sn(II) and Pb(II), being especially well-known due to their applicability in the design of efficient solar cells^{20–24}). Among the physical properties making HMs attractive from the point of view of materials science, there are photo-,^{25–27} thermo-,^{28–31} and solvatochromism,³² ferroelasticity,^{8,9} etc. Despite the low hydrolytic stability of group 15 halide complexes making them less convenient components of many composites or devices, they remain the focus of current research.

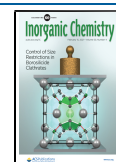
While synthetic approaches toward HMs are very straightforward,⁴ there exists a longstanding problem making this area especially attractive from the point of view of fundamental inorganic chemistry and crystal engineering: it is yet impossible to predict the structural type of an anion forming in a certain reaction. It is usually assumed that species of low nuclearity (most likely, mononuclear) exist in solution,³³ undergoing self-assembly into more complex units during the crystallization process, and this process is predominantly governed by the

nature of the cation³⁴ whose salt was used in synthesis. The more interesting fact is that relatively low energies of $\text{M}-\text{X}$ bonds and favorable ligand substitution kinetics in these systems enable the appearance of their unusual reactivity even in the solid state. A very spectacular example of this feature was presented by Mercier et al. over 12 years ago:³⁵ desolvation of a complex containing discrete $[\text{Bi}_4\text{I}_{16}]^{4-}$ anions resulted in dramatic changes in the molecular structure (formation of polymeric $\{[\text{Bi}_4]_n\}^{n-}$) in a single-crystal to single-crystal mode, and this process was reversible (!). A few examples describing the relationship between the number of solvent molecules and structural types³⁶ confirm the great lability in these systems.

In the course of our work aiming at the preparation and characterization of bromobismuthates(III),^{34,37,38} we decided to perform related experiments with bromoantimonates(III) in order to see whether stereochemically similar Bi(III) and Sb(III) would form complexes of the same structural type in the presence of the same organic cation. The outcome was unexpected: we found that initially there form deep orange

Received: December 18, 2020

Published: January 26, 2021



Cat[SbBr₅] (Cat = 1,1'-(1,2-ethanediyl)bis(pyridine) (PyC₂²⁺) (**1**) and 1,1'-(1,2-ethanediyl)bis(3,5-dimethylpyridine) (3,5-MePyC₂²⁺) (**2**), respectively, featuring an unusual pentacoordinated Sb and noncovalent Sb...Br contacts which, as described below, are believed to be responsible for the appearance of the unusual coloring. In the mother liquor, **1** transforms into (PyC₂)₂[Sb₂Br₁₀], which demonstrates polymorphism (**3** and **4**), while **2** transforms into the single-phase polymeric (3,5-MePyC₂)₂{[SbBr₄]}₂ (**5**).

EXPERIMENTAL SECTION

Starting Materials. All reagents were obtained from commercial sources and used as purchased. Solvents were purified according to the standard procedures. C₂PyBr₂ and (3,5-MePy)₂C₂Br₂ were obtained by reactions of 1,2-dibromoethane with pyridine or 3,5-dimethylpyridine, respectively (1:2.1, reflux, CH₃CN, 12 h), and identified by ¹H NMR spectra and elemental analysis.

Synthesis of 1–5. A 60 mg portion (0.2 mmol) of Sb₂O₃ was dissolved in 3 mL of concentrated HBr, followed by addition of C₂PyBr₂ (70 mg, 0.2 mmol) or (3,5-MePy)₂C₂Br₂ (70 mg, 0.2 mmol) in 3 mL of HBr. The mixtures were heated to 70 °C and slowly cooled to rt, resulting in deep orange crystals of **1** or **2**, respectively. After approximately 12 h in mother liquor, **1** and **2** transform into **3** (**4**) and **5**, respectively. Elemental analysis data are given in the Supporting Information.

X-ray Diffractometry. Single-crystal XRD data for **1**, **3**, and **5** were collected with an automated Agilent Xcalibur diffractometer equipped with an area AtlasS2 detector (graphite monochromator, λ(Mo Kα) = 0.71073 Å) (Table S1 in the Supporting Information). Integration and absorption correction were performed using the CrysAlisPro program package (CrysAlisPro 1.171.38.46, Rigaku Oxford Diffraction, 2015). Single-crystal XRD data for **2** were collected with a Bruker D8 Venture diffractometer with a CMOS PHOTON III detector and IμS 3.0 source (λ(Mo Kα) = 0.71073 Å). Absorption corrections were applied with the use of the SADABS program (Bruker Apex3 software suite: Apex3, SADABS-2016/2 and SAINT, version 2018.7-2; Bruker AXS Inc., Madison, WI, 2017). Single-crystal XRD data for **4** were collected with a Bruker Apex DUO diffractometer equipped with a 4K CCD area detector (graphite monochromator, λ(Mo Kα) = 0.71073 Å). Absorption corrections were applied with the use of the SADABS program (2000–2012), APEX2 (Version 2.0), SAINT (Version 8.18c), and SADABS (Version 2.11) (Bruker AXS Inc., Madison, WI). The crystal structures were solved using SHELXT³⁹ and were refined using SHELXL⁴⁰ with the OLEX2 GUI.⁴¹ Atomic thermal displacement parameters for non-hydrogen atoms were refined anisotropically. The somewhat high *R* factor and high residual electron density for structure **2** is due to the presence of a diffuse scattering along the *c** direction in *nkl* layers (Figure S1). This feature indicates some local ordering of adjacent columns of {SbBr₃}. CCDC 2026490–2026494 and 2051057 contain the supplementary crystallographic data for this paper. These data can be obtained free of charge via www.ccdc.cam.ac.uk/data_request/cif or by emailing data_request@ccdc.cam.ac.uk.

Differential Scanning Calorimetry (DSC). Thermal analysis was performed with a NETZSCH DSC 204 F1 Phoenix differential scanning calorimeter with a digital/discrete resolution of ~0.01 μW. DSC measurements were carried out by a heat flow measurement method at a 12–15 K min⁻¹ cooling/heating rate in 25 mL min⁻¹ Ar flux in unsealed aluminum crucibles with lids. Powdered samples were distributed uniformly over the bottom and carefully tamped. To increase the sensitivity and reduce baseline noise, measurements were taken at a heating rate of 12–15 K min⁻¹ without the supply of gas or liquid nitrogen (self-heating rate of the calorimeter cell ~10 K min⁻¹ at 130 K). The sensitivity of the sample carrier sensors and temperature scale gradation were calibrated by melting and crystal to crystal transition measurements of standard samples (cyclohexane, adamantane, Hg, Ga, benzoic acid, KNO₃, In).

Powder X-ray Diffractometry (PXRD). XRD analysis of polycrystals was performed on a Shimadzu XRD-7000 diffractometer

(Cu Kα radiation, Ni filter, linear One Sight detector, 5–50° 2θ range, 0.0143° 2θ step, 2 s per step). Polycrystalline samples were gently ground with hexane in an agate mortar, the resulting suspension was deposited on the polished side of a standard quartz sample holder, and a smooth thin layer was formed after drying. Experimentally obtained PXRD data and their comparison with calculated patterns are given in Supporting Information.

Computational Details, Thermogravimetric Analysis, and Diffuse Reflectance Spectroscopy. See the Supporting Information for details.

RESULTS AND DISCUSSION

For preparation of **1** and **2**, we used the general approach which is widely applied in HM chemistry:⁴ Sb₂O₃ was dissolved in HBr

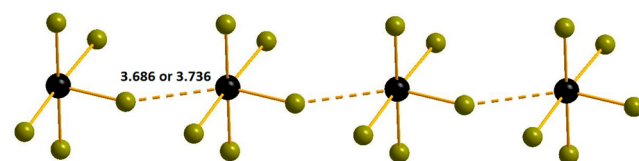


Figure 1. Supramolecular associates formed by [SbBr₅]²⁻ anions in the structures of **1** and **2**. Color code and definition here and below: Sb, black; Br, olive green; noncovalent contacts, dashed lines.

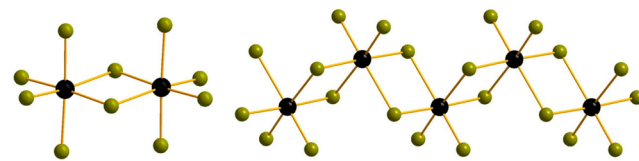


Figure 2. Structures of [Sb₂Br₁₀]⁴⁻ (left) and {[SbBr₄]_n}ⁿ⁻ (right) anions in **3** and **5**.

in order to generate bromoantimonate(III) species, followed by addition of an HBr solution of CatBr₂. Rapid isolation of **1** and **2** resulted in pure single-phase samples (see the Supporting Information for PRXD details: **1**, P1̄, *a* = 6.1343(3) Å, *b* = 9.2857(4) Å, *c* = 17.2041(9) Å, α = 90.331(4)°, β = 100.259(4)°, γ = 99.912(4)°, *Z* = 2; **2**, P2₁/*n*, *a* = 6.2898(4) Å, *b* = 8.7454(7) Å, *c* = 20.4076(16) Å, β = 90.438(3)°, *Z* = 2). In both cases, there are mononuclear [SbBr₅]²⁻ anions with pentacoordinated square-pyramidal Sb (examples of such bromoantimonates(III) were reported earlier, but those are rather uncommon³). The main structural feature of these structures is that, as follows from a comparison of Sb...Br distances (3.686 and 3.736 Å in **1** and **2**, respectively) with the sum of the corresponding van der Waals radii (3.89 Å^{42,43}), the existence of the corresponding noncovalent interactions between the neighboring [SbBr₅]²⁻ anions, resulting in the formation of supramolecular linear chains (Figure 1), can be assumed. In the case of **2**, the axial bromide ligand is disordered over two positions with 0.5/0.5 occupancy, arranging on either side of the {SbBr₄} plane. The disorder can be rationalized as follows. The [SbBr₅]²⁻ chains spread along the *a* axis; they are strictly ordered in this direction for stereochemical reasons. Along the *c* axis, there is a low probability of chains ordering, as indicated by the presence of diffuse scattering along the *c** axis in reciprocal space reconstructions (Figure S1). Along the *b* axis, the chains are either strictly ordered or randomly arranged: no diffuse scattering is observed in the corresponding reconstructions.

The ranges of Sb–Br distances in **1** and **2** are 2.547–2.838 and 2.580–2.813 Å, respectively. The shorter distances

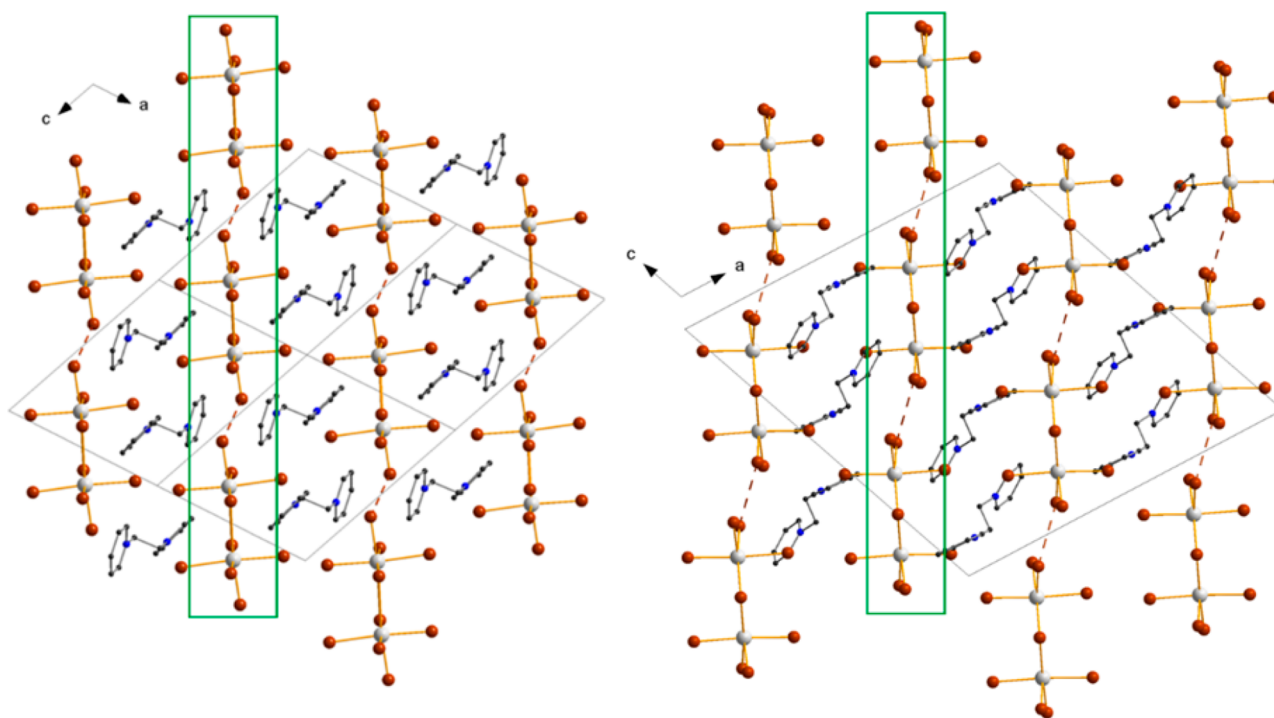


Figure 3. Crystal packings of **3** (left) and **4** (right). Green rectangles outline layers composed of $[\text{Sb}_2\text{Br}_{10}]^{4-}$. Hydrogen atoms are not shown. Dashed brown lines indicate shortened $\text{Br}\cdots\text{Br}$ contacts.

correspond to bromide ligands occupying the apex positions of the pyramids. The $\text{Sb}-\text{Br}\cdots\text{Sb}$ angles in the aforementioned $\{[\text{SbBr}_5]\}$ chains are 159.21 and 169.38° , respectively. In all cases, there are $\text{H}\cdots\text{Br}$ contacts between the cations and anions, which are common for halogenidometalates in general.³⁴

The samples of **1** and **2** start to transform into colorless solids within hours when they are kept in mother liquor; this process is completed overnight (it can be noted visually, and it is confirmed by PXRD data; see the [Supporting Information](#)). In both cases, it results in the formation of single crystals suitable for X-ray diffractometry, and the corresponding experiments were initially performed at low temperatures ([Table S1](#)), resulting in the determination of the structures of **3** and **5**, respectively. In **3** ($P\bar{1}$, $a = 10.1060(4)$ Å, $b = 10.2956(4)$ Å, $c = 11.1394(4)$ Å, $\alpha = 105.030(3)^\circ$, $\beta = 101.709(3)^\circ$, $\gamma = 117.233(4)^\circ$, $Z = 1$), the anionic part is represented by binuclear bromoantimonate(III) units $[\text{Sb}_2\text{Br}_{10}]^{4-}$ built of two edge-sharing octahedra ([Figure 2](#), left). This structural type is one of the most common in HMs of group 15 elements.^{3,44–47} The $\text{Sb}-\text{Br}_{\text{term}}$ and $\text{Sb}-\mu_2-\text{Br}$ distances are 2.570 – 2.855 and 2.872 – 3.333 Å, respectively. In **5** ($P2_1/n$, $a = 20.5536(8)$ Å, $b = 7.2974(2)$ Å, $c = 21.2510(7)$ Å, $\beta = 117.694(5)^\circ$, $Z = 4$), there are one-dimensional polymeric anions $\{[\text{SbBr}_4]_n\}^{n-}$ ([Figure 2](#), right) of type E according to a classification proposed by us earlier.⁴ The $\text{Sb}-\mu_2-\text{Br}$ bonds (2.727 – 3.183 Å) are elongated in comparison with $\text{Sb}-\text{Br}_{\text{term}}$ (2.581 – 2.622 Å); this is the usual effect for HMs.⁴

Attempting to prepare pure bulk samples of **3** and **5**, we noticed that, while **5** forms as a single phase (see the [Supporting Information](#)), experimental PXRD data for the substance which we expected to be **3** did not match to the XRD-based calculated pattern. This effect was persistent (over 10 reproductions), and the phase of **3** was fully absent, while elemental analysis data agreed with the composition of **3**. We assumed that this difference may be related to polymorphism. Indeed, we isolated

the crystals of the new phase **4** ($C2/c$, $a = 19.6880(8)$ Å, $b = 10.0152(5)$ Å, $c = 20.8410(9)$ Å, $\beta = 111.104(2)^\circ$, $Z = 4$) of higher symmetry (monoclinic vs triclinic in **3**) containing the same $[\text{Sb}_2\text{Br}_{10}]^{4-}$ anions. The crystal packings of compounds **3** and **4** are similar. Both compounds reveal layers of $[\text{Sb}_2\text{Br}_{10}]^{4-}$ spreading along the (-101) plane ([Figure 3](#)); the space between the layers is occupied by bis(pyridinium)ethane cations. In the layer of **3**, shortened $\text{Br}\cdots\text{Br}$ contacts (of 3.58 Å) are observed that connect anions in a chain ([Figure 4](#)). In the case of **4**, the corresponding distances are much longer (3.95 Å), which results in less dense packing: the anions in a van der Waals approximation occupy 31.5% of the cell volume in **4** vs 33.0% in **3**. Note that the cations also pack more densely in **3** (36.4% of the cell volume) in comparison to **4** (34.7%). Due to this, the crystal density of **3** is higher than that of **4** ([Table S1](#) in the [Supporting Information](#)).

In order to confirm or dismiss our hypothesis on thermally induced phase transitions between **3** and **4**, we performed an additional experiment: a single crystal of **4** was cooled to 130 K and an XRD analysis was performed again. Surprisingly, this did not lead to transformation into **3**; therefore, we cannot state that there is a single-crystal to single-crystal phase transition. In our opinion, this is rather the case of “common” polymorphism, but factors affecting the preferable formation of a certain polymorph are not clear.

According to DSC data ([Figure 5](#)), thermal anomalies associated with phase transitions were not detected in the 145 – 280 K range, confirming our XRD-based observations. Extended data on thermal stability (thermogravimetric analysis) are given in the [Supporting Information](#).

Diffuse reflectance spectra at room temperature for **1** and **4** are given in [Figures 6](#) and [7](#) (for **2** and **5**, these are presented in the [Supporting Information](#)). The spectra agree with the colors observed for these samples. For **1** and **2**, absorption edges are strongly shifted to longer wavelength ranges, resulting in

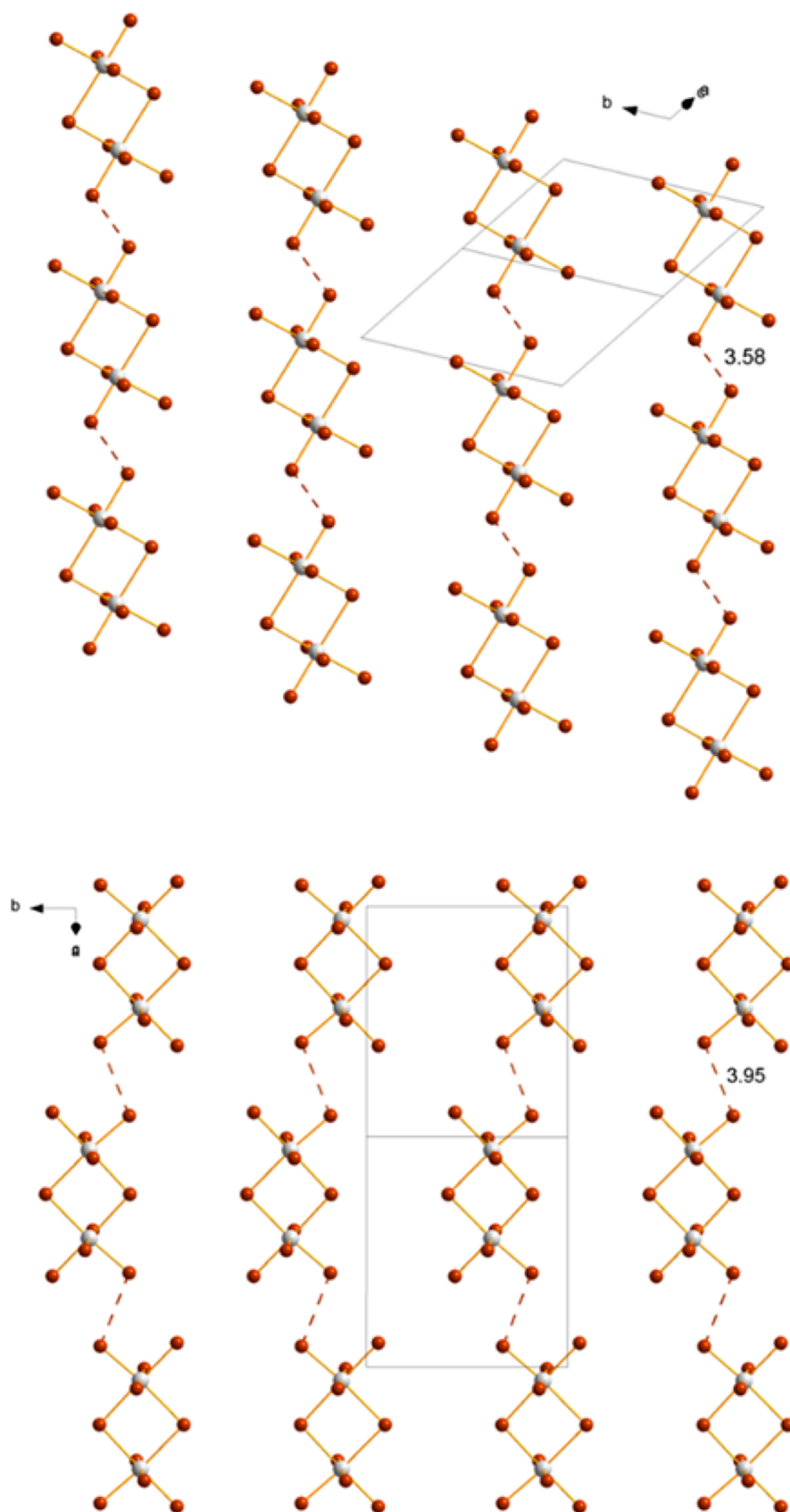


Figure 4. View of $[\text{Sb}_2\text{Br}_{10}]^{4-}$ layers in compounds **3** (top) and **4** (bottom). Dashed brown lines indicate shortened Br \cdots Br contacts.

noticeably narrower optical band gaps: for **1** and **2**, those are 2.28 and 2.17 eV, respectively, therefore being comparable with E_g values for iodoantimonates(III) of lower nuclearity.

In order to (1) investigate the nature of the aforementioned Sb \cdots Br noncovalent interactions in **1** and **2** and (2) see whether those could cause unusual changes in optical properties, we

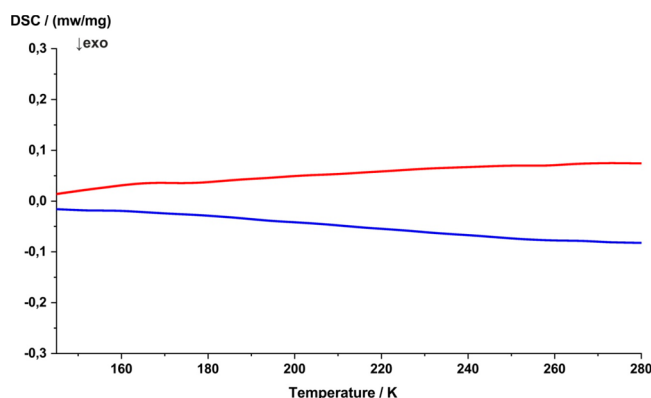


Figure 5. DSC curves for 4.

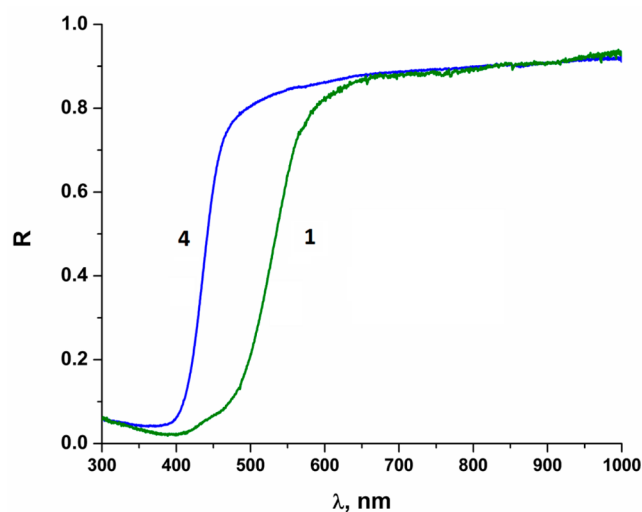


Figure 6. Diffuse reflectance spectra of 1 (green) and 4 (blue).

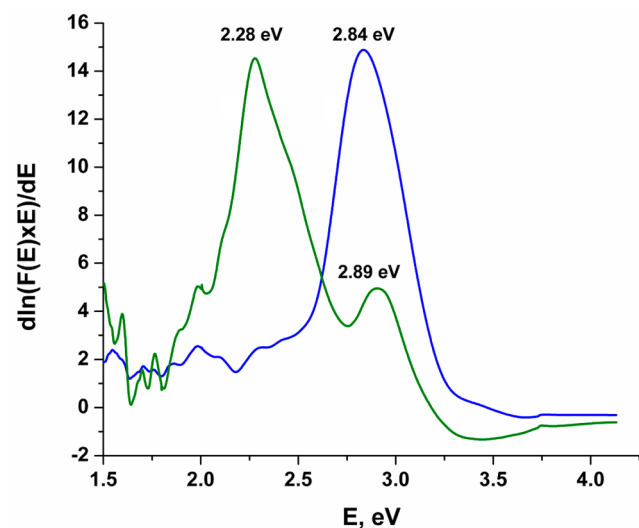
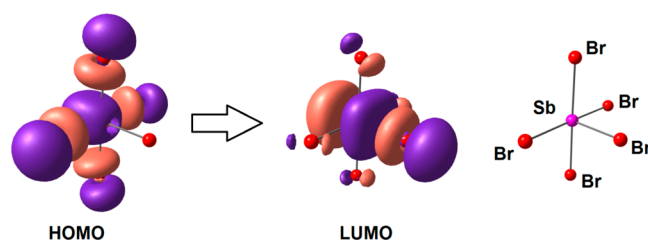
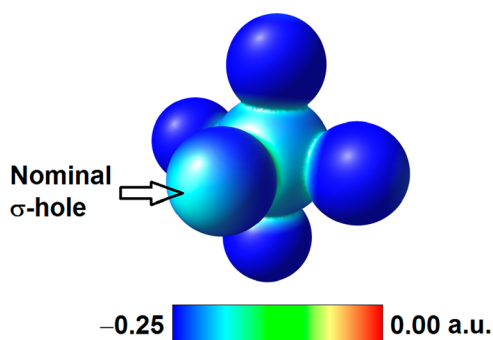


Figure 7. Diffuse reflectance spectra of 1 (green) and 4 (blue).

performed DFT calculations and a QTAIM-approach-based⁴⁸ analysis of the electron density distribution (see the [Experimental Section](#) for details). Unfortunately, we had to exclude 2 from these studies due to disorder. For comparison, we examined the structures of 3 and 5, and these results were rather unexpected ([Table 1](#)).

Figure 8. Frontier molecular orbitals in $[\text{SbBr}_5]^{2-}$ anion ($\omega\text{B97XD/DZP-DKH}$ level of theory).Figure 9. Electrostatic surface potential distribution in the $[\text{SbBr}_5]^{2-}$ anion ($\omega\text{B97XD/DZP-DKH}$ level of theory).

While the $\text{Sb}-\mu_2\text{-X}$ interactions are considered within the usual paradigm of coordination chemistry, the theoretical calculations within the QTAIM formalism contradict this idea: the low magnitude of the electron density, positive values of the Laplacian of electron density, and the balance between the potential and kinetic energy densities of electrons at the bond critical points (3, -1) for these “bonds” in 3 and 5 reveal that those indeed do have some very small covalent contribution,⁵⁰ but it is definitely not prominent (see [Figures S6–S8](#) in the Supporting Information for visualization). We believe that this fact is very interesting in terms of an understanding of halogenidometalate structural chemistry in general. The $\text{Sb}\cdots\text{Br}$ interactions in 1 are purely noncovalent.

In order to understand the influence of intermolecular interactions $\text{Sb}\cdots\text{Br}$ on the color of crystals 1 and 3, we carried out TD-DFT simulations of UV–vis absorption spectra for model mono-, di-, tri-, tetra-, penta-, and hexameric “oligomers” of 1 and monomeric and dimeric systems in the case of 3. Theoretical UV–vis absorption spectra for all of these model systems are shown in [Figures S9 and S10](#) in the Supporting Information. Obviously, the supramolecular organization and formation of chains due to $\text{Sb}\cdots\text{Br}$ intermolecular interactions lead to a shift in the simulated UV–vis absorption spectra to the long-wavelength region (the more such noncovalent contacts, the stronger the shift), which is collateral evidence that these $\text{Sb}\cdots\text{Br}$ intermolecular interactions can potentially influence the color of the crystals under study. In addition, an analysis of frontier molecular orbitals and the electrostatic surface potential distribution in the $[\text{SbBr}_5]^{2-}$ anion provides some additional insight into the reason for the dramatic difference in color of the studied crystals ([Figures 8 and 9](#)). Obviously, the infinite chains of $[\text{SbBr}_5]^{2-}$ anions can very easily transmit the electron density from the HOMO to the LUMO (in other words, using their nominal σ -holes) in the case where neighboring species are oriented in the same direction as in 1 and 2.

Table 1. Values of the Density of All Electrons ($\rho(r)$), Laplacian of Electron Density ($\nabla^2\rho(r)$) and Appropriate λ_2 Eigenvalues, Energy Density (H_b), Potential Energy Density ($V(r)$), and Lagrangian Kinetic Energy ($G(r)$) (au) at the Bond Critical Points (3, -1), Corresponding to Intermolecular Interactions Sb \cdots Br in 1, 3, and 5, Lengths of Appropriate Contacts (l , Å) and Estimated Strengths for These Interactions (E_{int} , kcal/mol)

structure	$\rho(r)$	$\nabla^2\rho(r)$	λ_2	H_b	$V(r)$	$G(r)$	l	E_{int}^a	E_{int}^b
1	0.008	0.021	-0.008	0.001	-0.004	0.005	3.686	1.5	1.8
3	0.018	0.035	-0.018	-0.001	-0.010	0.009	3.333	3.6	3.2
5	0.019	0.034	-0.019	-0.001	-0.010	0.009	3.290	3.6	3.2

$^a E_{\text{int}} = 0.58(-V(r))$ (this empirical correlation between the interaction energy and the potential energy density of electrons at the bond critical points (3, -1) was specifically developed for noncovalent interactions involving bromine atoms).⁴⁹ $^b E_{\text{int}} = 0.57(G(r))$ (this empirical correlation between the interaction energy and the kinetic energy density of electrons at the bond critical points (3, -1) was specifically developed for noncovalent interactions involving bromine atoms).⁴⁹

CONCLUSIONS

There are two important points which can be highlighted as conclusions. First, we confirmed that noncovalent interactions can have a large influence on the optical properties of halogenidometalates. These observations agree well with our earlier results for bromobismuthates⁵¹ (in that case, the unusual coloring was caused by cation \cdots anion halogen bonding), and this allows us to assume that it can be utilized for directed tuning of the properties of halogenidometalate-based materials (e.g., light absorbers in solar cells or photodetectors). Second, DFT calculations reveal that the nature of metal \cdots halogen interactions in halogenidometalates can be different from what it is commonly used to be—most likely, some “metal–halogen bonds” should rather be considered within a supramolecular paradigm. In our opinion, this “provocative” statement requires a special investigation involving an extended set of halogenidometalate structural data. Corresponding research is underway in our group.

ASSOCIATED CONTENT

Supporting Information

The Supporting Information is available free of charge at <https://pubs.acs.org/doi/10.1021/acs.inorgchem.0c03699>.

XRD, diffuse reflectance spectroscopy, computational details, and PXRD data (PDF)

Accession Codes

CCDC 2026490–2026494 and 2051057 contain the supplementary crystallographic data for this paper. These data can be obtained free of charge via www.ccdc.cam.ac.uk/data_request/cif, or by emailing data_request@ccdc.cam.ac.uk, or by contacting The Cambridge Crystallographic Data Centre, 12 Union Road, Cambridge CB2 1EZ, UK; fax: +44 1223 336033.

AUTHOR INFORMATION

Corresponding Author

Sergey A. Adonin – Nikolaev Institute of Inorganic Chemistry SB RAS, 630090 Novosibirsk, Russia; South Ural State University, 454080 Chelyabinsk, Russia; orcid.org/0000-0002-9889-5273; Email: adonin@niic.nsc.ru

Authors

Andrey N. Usoltsev – Nikolaev Institute of Inorganic Chemistry SB RAS, 630090 Novosibirsk, Russia

Taisiya S. Sukhikh – Nikolaev Institute of Inorganic Chemistry SB RAS, 630090 Novosibirsk, Russia; orcid.org/0000-0001-5269-9130

Alexander S. Novikov – Saint Petersburg State University, 199034 Saint Petersburg, Russia; orcid.org/0000-0001-9913-5324

Vladimir R. Shayapov – Nikolaev Institute of Inorganic Chemistry SB RAS, 630090 Novosibirsk, Russia

Denis P. Pishchur – Nikolaev Institute of Inorganic Chemistry SB RAS, 630090 Novosibirsk, Russia; orcid.org/0000-0002-0532-6478

Ilya V. Korolkov – Nikolaev Institute of Inorganic Chemistry SB RAS, 630090 Novosibirsk, Russia

Ilyas F. Sakhapov – South Ural State University, 454080 Chelyabinsk, Russia

Vladimir P. Fedin – Nikolaev Institute of Inorganic Chemistry SB RAS, 630090 Novosibirsk, Russia

Maxim N. Sokolov – Nikolaev Institute of Inorganic Chemistry SB RAS, 630090 Novosibirsk, Russia; orcid.org/0000-0001-9361-4594

Complete contact information is available at:

<https://pubs.acs.org/doi/10.1021/acs.inorgchem.0c03699>

Author Contributions

The manuscript was written through contributions of all authors. All authors have given approval to the final version of the manuscript.

Funding

This work was supported by the Russian Science Foundation (Grant No. 18-73-10040).

Notes

The authors declare no competing financial interest.

REFERENCES

- Werner, A. Beitrag Zur Konstitution Anorganischer Verbindungen. *Z. Anorg. Chemie* **1893**, 3 (1), 267–330.
- Wu, L.-M.; Wu, X.-T.; Chen, L. Structural Overview and Structure–property Relationships of Iodoplumbate and Iodobismuthate. *Coord. Chem. Rev.* **2009**, 253 (23–24), 2787–2804.
- Fisher, G. A.; Norman, N. C. The Structures of the Group 15 Element(III) Halides and Halogenoanions. *Adv. Inorg. Chem.* **1994**, 41, 233–271.
- Adonin, S. A.; Sokolov, M. N.; Fedin, V. P. Polynuclear Halide Complexes of Bi(III): From Structural Diversity to the New Properties. *Coord. Chem. Rev.* **2016**, 312, 1.
- Adonin, S. A.; Sokolov, M. N.; Fedin, V. P. Bismuth(III) Halide Complexes: New Structural Types and New Application Areas. *Russ. J. Inorg. Chem.* **2017**, 62 (14), 1789.
- Sharutin, V. V.; Egorova, I. V.; Klepikov, N. N.; Boyarkina, E. A.; Sharutina, O. K. Synthesis and Structure of Bismuth Complexes [Ph₃MeP] 2 + [BiI_{3.5}Br_{1.5}(C₅H₅N)]₂ · C₅H₅N, [Ph₄ Bi] 4 + [Bi₄I₁₆] 4 · 2Me₂C=O, and [Ph₃(Iso-Am)P] 4 + [Bi₈I₂₈] 4 · 2Me₂C=O. *Russ. J. Inorg. Chem.* **2009**, 54 (11), 1768–1778.

- (7) Krautscheid, H. Synthese Und Kristallstrukturen von (Ph₄P)₄[Bi₈I₂₈], (NBu₄N)[Bi₂I₇] Und (Et₃PhN)₂[Bi₃I₁₁] - Iodobismutate Mit Isolierten Bzw. Polymeren Anionen. *Z. Anorg. Allg. Chem.* **1995**, *621* (12), 2049–2054.
- (8) Wojtaś, M.; Jakubas, R.; Baran, J. Vibrational Study of the Ferroelastic Phase Transition in [(CH₃)₄P]₃[Bi₂Cl₉] and [(CH₃)₄P]₃[Bi₂Br₉]. *Vib. Spectrosc.* **2005**, *39* (1), 23–30.
- (9) Wojtaś, M.; Jakubas, R.; Ciunik, Z.; Medycki, W. Structure and Phase Transitions in [(CH₃)₄P]₃[Sb₂Br₉] and [(CH₃)₄P]₃[Bi₂Br₉]. *J. Solid State Chem.* **2004**, *177* (4–5), 1575–1584.
- (10) Kulicka, B.; Lis, T.; Kinzhybalov, V.; Jakubas, R.; Piecha, A. Novel Anionic Water-Containing Inorganic Fragment in [4-NH₂PyH]₈[Bi₂Cl₁₁][Bi₂Cl₉(H₂O)₂]: Structural Characterization, Thermal, Dielectric and Vibrational Properties. *Polyhedron* **2010**, *29* (8), 2014–2022.
- (11) Piecha, A.; Jakubas, R.; Kinzhybalov, V.; Medycki, W. Crystal Structure, Dielectric Properties and Molecular Motions of Molecules in Thiazolium Halometalates(III): (C₃H₄NS)₆M₄Br₁₈·2H₂O (M = Sb, Bi). *J. Mol. Struct.* **2012**, *1013*, 55–60.
- (12) Krautscheid, H.; Vielsack, F. [Pb₁₈I₄₄]₈—An Iodoplumbate with an Unusual Structure. *Angew. Chem., Int. Ed. Engl.* **1995**, *34* (18), 2035–2037.
- (13) Heine, J. A Step Closer to the Binary: The 1∞[Bi₆I₂₀]²⁻ Anion. *Dalt. Trans.* **2015**, *44* (21), 10069–10077.
- (14) Dehnhardt, N.; Klement, P.; Chatterjee, S.; Heine, J. Divergent Optical Properties in an Isomorphous Family of Multinary Iodido Pentalates. *Inorg. Chem.* **2019**, *58* (16), 10983–10990.
- (15) Dehnhardt, N.; Borkowski, H.; Schepp, J.; Tonner, R.; Heine, J. Ternary Iodido Bismuthates and the Special Role of Copper. *Inorg. Chem.* **2018**, *57* (2), 633–640.
- (16) Ouasri, A.; Rhandour, A.; Saadi, M.; El Ammari, L. Catena-Poly[Heptylenediammonium [[Tetrachloridobismuthate(III)]-μ-Chlorido]]. *Acta Crystallogr. Sect. E Struct. Reports Online* **2013**, *69* (8), m437–m437.
- (17) Ouasri, A.; Jegnou, H.; Rhandour, A.; Roussel, P. Structures and Phases Transition in Hexylenediammonium Pentachlorobismuthate (III) [NH₃(CH₂)₆NH₃][BiCl₅] Crystal. *J. Solid State Chem.* **2013**, *200*, 22–29.
- (18) Dehnhardt, N.; Paneth, H.; Hecht, N.; Heine, J. Multinary Halogenido Bismuthates beyond the Double Perovskite Motif. *Inorg. Chem.* **2020**, *59*, 3394–3405.
- (19) Frolova, L. A.; Anokhin, D. V.; Piryazev, A. A.; Luchkin, S. Y.; Dremova, N. N.; Troshin, P. A. Exploring the Photovoltaic Performance of All-Inorganic Ag₂PbI₄/PbI₂ Blends. *J. Phys. Chem. Lett.* **2017**, *8* (7), 1651–1656.
- (20) Leblanc, A.; Mercier, N.; Allain, M.; Dittmer, J.; Pauporté, T.; Fernandez, V.; Boucher, F.; Kepenekian, M.; Katan, C. Enhanced Stability and Band Gap Tuning of α-[HC(NH₂)₂]₂PbI₃ Hybrid Perovskite by Large Cation Integration. *ACS Appl. Mater. Interfaces* **2019**, *11* (23), 20743–20751.
- (21) Leblanc, A.; Mercier, N.; Allain, M.; Dittmer, J.; Fernandez, V.; Pauporté, T. Lead- and Iodide-Deficient (CH₃NH₃)₃PbI₃ (D-MAPI): The Bridge between 2D and 3D Hybrid Perovskites. *Angew. Chem., Int. Ed.* **2017**, *56* (50), 16067–16072.
- (22) Belich, N. A.; Tychinina, A. S.; Kuznetsov, V. V.; Goodilin, E. A.; Grätzel, M.; Tarasov, A. B. Template Synthesis of Methylammonium Lead Iodide in the Matrix of Anodic Titanium Dioxide via the Direct Conversion of Electrodeposited Elemental Lead. *Mendeleev Commun.* **2018**, *28* (5), 487–489.
- (23) Fateev, S. A.; Petrov, A. A.; Khrustalev, V. N.; Dorovatovskii, P. V.; Zubavichus, Y. V.; Goodilin, E. A.; Tarasov, A. B. Solution Processing of Methylammonium Lead Iodide Perovskite from γ-Butyrolactone: Crystallization Mediated by Solvation Equilibrium. *Chem. Mater.* **2018**, *30* (15), 5237–5244.
- (24) Frolova, L. A.; Anokhin, D. V.; Piryazev, A. A.; Luchkin, S. Y.; Dremova, N. N.; Stevenson, K. J.; Troshin, P. A. Highly Efficient All-Inorganic Planar Heterojunction Perovskite Solar Cells Produced by Thermal Coevaporation of CsI and PbI₂. *J. Phys. Chem. Lett.* **2017**, *8* (1), 67–72.
- (25) Wang, Y.-L.; Chen, X.-H.; Shu, W.; Qin, H.-G.; Lin, J.-D.; Lin, R.-G.; Wen, N. Synthesis, Crystal Structure and Photochromic Property of a Phenethyl Viologen Bismuth(III) Chloride. *J. Coord. Chem.* **2019**, *72* (4), 573–583.
- (26) Xu, G.; Guo, G.-C.; Wang, M.-S.; Zhang, Z.-J.; Chen, W.-T.; Huang, J.-S. Photochromism of a Methyl Viologen Bismuth(III) Chloride: Structural Variation Before and After UV Irradiation. *Angew. Chem., Int. Ed.* **2007**, *46* (18), 3249–3251.
- (27) Lin, R.-G.; Xu, G.; Wang, M.-S.; Lu, G.; Li, P.-X.; Guo, G.-C. Improved Photochromic Properties on Viologen-Based Inorganic–Organic Hybrids by Using π-Conjugated Substituents as Electron Donors and Stabilizers. *Inorg. Chem.* **2013**, *52* (3), 1199–1205.
- (28) Zhang, W.; Sun, Z.; Zhang, J.; Han, S.; Ji, C.; Li, L.; Hong, M.; Luo, J. Thermochromism to Tune the Optical Bandgap of a Lead-Free Perovskite-Type Hybrid Semiconductor for Efficiently Enhancing Photocurrent Generation. *J. Mater. Chem. C* **2017**, *5* (38), 9967–9971.
- (29) Gağor, A.; Węclawik, M.; Bondzior, B.; Jakubas, R. Periodic and Incommensurately Modulated Phases in a (2-Methylimidazolium)-Tetraiodobismuthate(III) Thermochromic Organic–inorganic Hybrid. *CrystEngComm* **2015**, *17* (17), 3286–3296.
- (30) Bukvetskii, B. V.; Sedakova, T. V.; Mirochnik, A. G. Crystal Structure and Luminescence and Thermochromic Properties of Bis-1,10-Phenanthroline Hexachlorotellurate(IV). *Russ. J. Coord. Chem.* **2012**, *38* (2), 106–110.
- (31) Bukvetskii, B. V.; Sedakova, T. V.; Mirochnik, A. G. Crystal Structure, Luminescence, and Thermochromic Properties of Bis-(Tetraethylammonium) Hexabromotellurate(IV). *Russ. J. Inorg. Chem.* **2011**, *56* (2), 213–217.
- (32) Wagner, B.; Dehnhardt, N.; Schmid, M.; Klein, B. P.; Ruppenthal, L.; Müller, P.; Zugermeier, M.; Gottfried, J. M.; Lippert, S.; Halbich, M.-U.; et al. Color Change Effect in an Organic–Inorganic Hybrid Material Based on a Porphyrin Diacid. *J. Phys. Chem. C* **2016**, *120* (49), 28363–28373.
- (33) Mercier, N.; Louvain, N.; Bi, W. Structural Diversity and Retro-Crystal Engineering Analysis of Iodometalate Hybrids. *CrystEngComm* **2009**, *11* (5), 720.
- (34) Adonin, S. A.; Gorokh, I. D.; Novikov, A. S.; Samsonenko, D. G.; Korolkov, I. V.; Sokolov, M. N.; Fedin, V. P. Bromobismuthates: Cation-Induced Structural Diversity and Hirshfeld Surface Analysis of Cation–anion Contacts. *Polyhedron* **2018**, *139*, 282.
- (35) Bi, W.; Mercier, N. Reversible Dynamic Isomerism Change in the Solid State, from Bi₄I₁₆ Clusters to Bi₄ 1D Chains in l-Cystine Based Hybrids: Templating Effect of Cations in Iodobismuthate Network Formation. *Chem. Commun.* **2008**, *0* (44), 5743.
- (36) Goforth, A. M.; Peterson, L. R.; Smith, M. D.; Zur Loye, H. C. Syntheses and Crystal Structures of Several Novel Alkylammonium Iodobismuthate Materials Containing the 1,3-Bis-(4-Piperidinium)-Propane Cation. *J. Solid State Chem.* **2005**, *178* (11), 3529–3540.
- (37) Adonin, S. A.; Rakhmanova, M. I.; Samsonenko, D. G.; Sokolov, M. N.; Fedin, V. P. Hybrid Salts of Binuclear Bi(III) Halide Complexes with 1,2-Bis(Pyridinium)Ethane Cation: Synthesis, Structure and Luminescent Behavior. *Inorg. Chim. Acta* **2016**, *450*, 232.
- (38) Adonin, S. A.; Gorokh, I. D.; Novikov, A. S.; Usoltsev, A. N.; Sokolov, M. N.; Fedin, V. P. Tetranuclear Anionic Bromobismuthate [Bi₄Br₁₈]⁶⁻: New Structural Type in Halometalate Collection. *Inorg. Chem. Commun.* **2019**, *103*, 72–74.
- (39) Sheldrick, G. M. SHELXT – Integrated Space-Group and Crystal-Structure Determination. *Acta Crystallogr., Sect. A: Found. Adv.* **2015**, *71* (1), 3–8.
- (40) Sheldrick, G. M.; IUCr. Crystal Structure Refinement with SHELXL. *Acta Crystallogr., Sect. C: Struct. Chem.* **2015**, *71* (1), 3–8.
- (41) Dolomanov, O. V.; Bourhis, L. J.; Gildea, R. J.; Howard, J. A. K.; Puschmann, H. OLEX2: A Complete Structure Solution, Refinement and Analysis Program. *J. Appl. Crystallogr.* **2009**, *42* (2), 339–341.
- (42) Bondi, A. Van Der Waals Volumes and Radii of Metals in Covalent Compounds. *J. Phys. Chem.* **1966**, *70* (9), 3006–3007.
- (43) Mantina, M.; Chamberlin, A. C.; Valero, R.; Cramer, C. J.; Truhlar, D. G. Consistent van Der Waals Radii for the Whole Main Group. *J. Phys. Chem. A* **2009**, *113* (19), 5806–5812.

(44) Terao, H.; Ninomiya, S.; Hashimoto, M.; Eda, K. 81Br NQR and Crystal Structure of 4-Bromopyridinium Pentabromoantimonate(III); 3c–4e Bonding and NQR Trans Influence. *J. Mol. Struct.* **2010**, *965* (1–3), 68–73.

(45) Piecha, A.; Kinzhyalo, V.; Jakubas, R.; Baran, J.; Medycki, W. Structural Characterization, Molecular Dynamics, Dielectric and Spectroscopic Properties of Tetrakis(Pyrazolium) Bis(M2-Bromo-Tetrabromobismuthate(III)) Dihydrate, [C₃N₂H₅]₄[Bi₂Br₁₀]·2H₂O. *Solid State Sci.* **2007**, *9* (11), 1036–1048.

(46) Kotov, V. Y.; Ilyukhin, A. B.; Simonenko, N. P.; Kozyukhin, S. A. Synthesis, Thermal Stability, Crystal Structure and Optical Properties of 1,1'-(1,n-Alkanediyl)Bis(4-Methylpyridinium) Bromobismuthates. *Polyhedron* **2017**, *137*, 122–126.

(47) Wang, Y. K.; Wu, Y. L.; Lin, X. Y.; Wang, D. H.; Zhang, W. T.; Song, K. Y.; Li, H. H.; Chen, Z. R. Halobismuthate/Diphenyliodonium Hybrids Stabilized by Secondary Hypervalent I(III)···X Interactions: Structures, Optical Studies and Thermochromisms. *J. Mol. Struct.* **2018**, *1151*, 81–87.

(48) Bader, R. F. W. A Quantum Theory of Molecular Structure and Its Applications. *Chem. Rev.* **1991**, *91* (5), 893–928.

(49) Bartashevich, E. V.; Tsirelson, V. G. Interplay between Non-Covalent Interactions in Complexes and Crystals with Halogen Bonds. *Russ. Chem. Rev.* **2014**, *83* (12), 1181–1203.

(50) Espinosa, E.; Alkorta, I.; Elguero, J.; Molins, E. From Weak to Strong Interactions: A Comprehensive Analysis of the Topological and Energetic Properties of the Electron Density Distribution Involving X–H···F–Y Systems. *J. Chem. Phys.* **2002**, *117* (12), 5529–5542.

(51) Adonin, S. A.; Gorokh, I. D.; Novikov, A. S.; Abramov, P. A.; Sokolov, M. N.; Fedin, V. P. Halogen Contacts-Induced Unusual Coloring in Bi^{III}Bromide Complex: Anion-to-Cation Charge Transfer via Br···Br Interactions. *Chem. - Eur. J.* **2017**, *23* (62), 15612.